Thermally invisible sensors

Liujun Xu[1(a)] [ID], Jipeng Huang[1], Tao Jiang[2], Long Zhang[3] and Jiping Huang[1(b)]

[1] *Department of Physics, State Key Laboratory of Surface Physics, and Key Laboratory of Micro and Nano Photonic Structures (MOE), Fudan University - Shanghai 200438, China*
[2] *Department of Radiology, Changhai Hospital, Naval Medical University - Shanghai 200433, China*
[3] *Key Laboratory of Materials for High-Power Laser, Shanghai Institute of Optics and Fine Mechanics,*
Chinese Academy of Sciences - Shanghai 201800, China

Abstract – Accurate temperature detection requires a thermal sensor with high performance. In general, once a thermal sensor is placed in a temperature field, it will distort the temperature field more or less. Therefore, the thermal sensor is inaccurate and thermally visible, which constitutes an issue in many practical applications. Here we propose a bilayer scheme to maintain the original temperatures in both sensor and matrix, yielding an accurate and thermally invisible sensor. By solving the linear Laplace equation (with temperature-independent thermal conductivity), we derive two groups of thermal conductivities to realize thermally invisible sensors, even considering geometrically anisotropic cases. These results can be directly extended to thermally nonlinear cases (with temperature-dependent thermal conductivity), as long as the ratio between the nonlinear thermal conductivities of sensor and matrix is a temperature-independent constant. These explorations are beneficial to temperature detection and provide insights into thermal camouflage.

Introduction. – Precision measurement is indispensable in many fields, so high-performance sensors become crucially important. Generally, when a sensor is put in a physical field, it will distort the physical field more or less. Therefore, the measured value is actually not the original one, thus making the sensor inaccurate. In addition to inaccuracy, the perturbation resulted from the sensor itself also makes the sensor "visible", which constitutes an issue in many practical applications. To solve the problem, the methods of scattering cancellation [1] and transformation optics [2] were proposed to design electromagnetically invisible sensors. Acoustically invisible sensors [3–5] and magnetically invisible sensors [6] were also proposed successively.

Thermally invisible sensors also attracted research interest. The methods of scattering cancellation [7–9], neutral inclusion [10], and transformation thermotics [11] were put forward to design thermally invisible sensors. To go further, a multiphysically invisible sensor was also fabricated

for both thermal and electrical detections [12]. These studies paid main attention to thermal invisibility because it is particularly important to hinder infrared detection. For example, when a thermal sensor is detecting temperature, invisibility can protect the sensor itself from being discovered. However, accuracy is almost neglected in these schemes, so the detected temperature has deviations from the original one, thus making thermal sensors inaccurate. Meanwhile, thermally invisible sensors for nonlinear cases are still lacking, which also limits practical applications. Here, "nonlinear" means that thermal conductivities are temperature-dependent.

To solve the problem, here we propose a bilayer scheme to design thermally invisible sensors, even considering geometrically anisotropic cases and thermally nonlinear cases. These two points are beneficial to practical applications because thermal sensors do not have to be geometrically isotropic and nonlinear thermal conductivities are common in nature. In fact, the bilayer scheme has achieved great success in designing thermal cloaks [13–17], thermal concentrators [18], and chameleon-like metashells [19,20]. Essentially, cloaks make the temperature gradient in

(a)E-mail: 13307110076@fudan.edu.cn
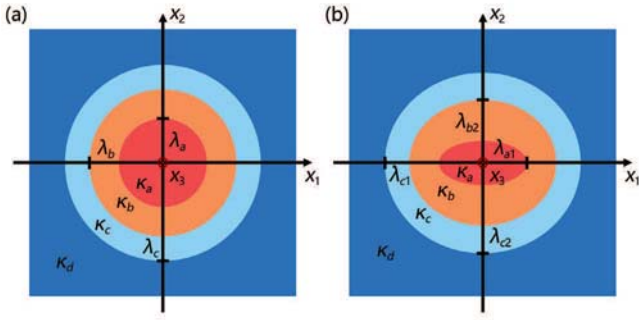(b)E-mail: jphuang@fudan.edu.cn

Fig. 1: Schematic diagrams of (a) geometrically isotropic case and (b) geometrically anisotropic case.

the center be zero; concentrators make the temperature gradient in the center steeper than that in the matrix; and invisible sensors keep the same temperature gradient in the sensor and matrix. By solving the linear Laplace equation, we derive two groups of thermal conductivities to make thermal sensors both accurate and invisible. Moreover, we prove that the bilayer scheme can be directly extended to thermally nonlinear cases as long as the ratio between the nonlinear thermal conductivities of sensor and matrix is a temperature-independent constant.

Linear thermotics: geometrically isotropic case.
– We discuss the case shown in fig. 1(a). The Cartesian coordinates are denoted as x_i ($i = 1$, 2 for two dimensions and $i = 1$, 2, 3 for three dimensions). The radii of the core, inner shell, and outer shell are denoted as λ_a, λ_b, and λ_c, respectively. The thermal conductivities of the core, inner shell, outer shell, and matrix are denoted as κ_a, κ_b, κ_c, and κ_d, respectively. Since the geometry is isotropic, we discuss the case in cylindrical coordinates (r, θ) or spherical coordinates (r, θ, φ). Here, two dimensions and three dimensions are similar because φ essentially does not matter. In the presence of an external linear thermal field $\boldsymbol{G}_0$, the temperature profiles in different regions can be expressed as

$$T_a = u_a r \cos\theta, \tag{1a}$$
$$T_b = (u_b r + v_b r^{-\tau})\cos\theta, \tag{1b}$$
$$T_c = (u_c r + v_c r^{-\tau})\cos\theta, \tag{1c}$$
$$T_d = (u_d r + v_d r^{-\tau})\cos\theta, \tag{1d}$$

where T_a, T_b, T_c, and T_d are the temperatures in the core, inner shell, outer shell, and matrix, respectively. $\tau = 1$ for two dimensions and $\tau = 2$ for three dimensions. u_a, u_b, v_b, u_c, v_c, u_d, and v_d are seven coefficients to be determined by the following boundary conditions:

$$u_a\lambda_a = u_b\lambda_a + v_b\lambda_a^{-\tau}, \tag{2a}$$
$$u_b\lambda_b + v_b\lambda_b^{-\tau} = u_c\lambda_b + v_c\lambda_b^{-\tau}, \tag{2b}$$
$$u_c\lambda_c + v_c\lambda_c^{-\tau} = u_d\lambda_c + v_d\lambda_c^{-\tau}, \tag{2c}$$
$$\kappa_a u_a = \kappa_b(u_b - \tau v_b\lambda_a^{-\tau-1}), \tag{2d}$$

$$\kappa_b(u_b - \tau v_b\lambda_b^{-\tau-1}) = \kappa_c(u_c - \tau v_c\lambda_b^{-\tau-1}), \tag{2e}$$
$$\kappa_c(u_c - \tau v_c\lambda_c^{-\tau-1}) = \kappa_d(u_d - \tau v_d\lambda_c^{-\tau-1}), \tag{2f}$$
$$u_d = G_0, \tag{2g}$$
$$v_d = 0, \tag{2h}$$
$$u_a = u_d. \tag{2i}$$

Equations (2a)–(2c) and (2d)–(2f) indicate the continuities of temperature and heat flux, respectively. Equations (2g) and (2h) ensure a linear thermal field in the matrix, thus making the sensor thermally invisible. Equation (2i) makes the temperature in the sensor the same as that in the matrix, thus ensuring accurate detection. We take κ_b and κ_c as other two coefficients which (together with the seven coefficients in eqs. (1a)–(1d)) can be determined by the nine equations in eq. (2). Therefore, κ_b and κ_c can be solved as

$$\kappa_b^{(1)} = \frac{\kappa_a\alpha_3 - \kappa_d\alpha_1 + \sqrt{(\kappa_a - \kappa_d)(\kappa_a\alpha_2^2 - \kappa_d\alpha_1^2)}}{\alpha_5},$$
$$\tag{3a}$$
$$\kappa_c^{(1)} = \frac{\kappa_a\alpha_2 - \kappa_d\alpha_4 - \sqrt{(\kappa_a - \kappa_d)(\kappa_a\alpha_2^2 - \kappa_d\alpha_1^2)}}{\alpha_6},$$
$$\tag{3b}$$

or

$$\kappa_b^{(2)} = \frac{\kappa_a\alpha_3 - \kappa_d\alpha_1 - \sqrt{(\kappa_a - \kappa_d)(\kappa_a\alpha_2^2 - \kappa_d\alpha_1^2)}}{\alpha_5},$$
$$\tag{4a}$$
$$\kappa_c^{(2)} = \frac{\kappa_a\alpha_2 - \kappa_d\alpha_4 + \sqrt{(\kappa_a - \kappa_d)(\kappa_a\alpha_2^2 - \kappa_d\alpha_1^2)}}{\alpha_6},$$
$$\tag{4b}$$

where

$$\begin{aligned}\alpha_1 &= \lambda_a^{1+\tau}(\lambda_b^{1+\tau} + \tau\lambda_c^{1+\tau}) \\ &\quad + \lambda_b^{1+\tau}[\tau\lambda_b^{1+\tau} - (2\tau+1)\lambda_c^{1+\tau}],\end{aligned} \tag{5a}$$
$$\begin{aligned}\alpha_2 &= \lambda_a^{1+\tau}[(2\tau+1)\lambda_b^{1+\tau} - \tau\lambda_c^{1+\tau}] \\ &\quad - \lambda_b^{1+\tau}(\tau\lambda_b^{1+\tau} + \lambda_c^{1+\tau}),\end{aligned} \tag{5b}$$
$$\begin{aligned}\alpha_3 &= \lambda_a^{1+\tau}[2\tau\lambda_a^{1+\tau} - (2\tau-1)\lambda_b^{1+\tau} - \tau\lambda_c^{1+\tau}] \\ &\quad + \lambda_b^{1+\tau}(\tau\lambda_b^{1+\tau} - \lambda_c^{1+\tau}),\end{aligned} \tag{5c}$$
$$\begin{aligned}\alpha_4 &= \lambda_b^{1+\tau}(\lambda_a^{1+\tau} - \tau\lambda_b^{1+\tau}) \\ &\quad + \lambda_c^{1+\tau}[\tau\lambda_a^{1+\tau} + (2\tau-1)\lambda_b^{1+\tau} - 2\tau\lambda_c^{1+\tau}],\end{aligned} \tag{5d}$$
$$\alpha_5 = 2\tau(\lambda_a^{1+\tau} - \lambda_b^{1+\tau})(\lambda_a^{1+\tau} - \lambda_c^{1+\tau}), \tag{5e}$$
$$\alpha_6 = 2\tau(\lambda_a^{1+\tau} - \lambda_c^{1+\tau})(\lambda_b^{1+\tau} - \lambda_c^{1+\tau}). \tag{5f}$$

When $\kappa_a < \kappa_d$, eqs. (3) and (4) are always positive. When $\kappa_a = \kappa_d$, the sensor has the same thermal conductivity as the matrix, resulting in $\kappa_b = \kappa_c = \kappa_a = \kappa_d$, so the bilayer scheme is not necessary. When $\kappa_a > \kappa_d$, eqs. (3b) and (4a) are negative. Negative thermal conductivity means that the direction of heat flux is from low temperature to high temperature, which can be effectively realized by introducing extra energy [21]. Also, we do not need to worry

about complex values as long as the value of λ_b is appropriately chosen. Physically speaking, when $\kappa_a < \kappa_d$, the temperature gradient in the sensor is larger than that in the matrix, and the bilayer scheme can reduce temperature gradient to make the temperature gradients in the sensor and matrix the same; when $\kappa_a > \kappa_d$, the temperature gradient in the sensor is smaller than that in the matrix, but the bilayer scheme cannot enhance temperature gradient with only positive thermal conductivities.

Linear thermotics: geometrically anisotropic case. – We discuss the case shown in fig. 1(b). The semi-axes of the core, inner shell, and outer shell are denoted as λ_{ai}, λ_{bi}, and λ_{ci}, respectively ($i = 1, 2$ for two dimensions and $i = 1, 2, 3$ for three dimensions). Since the geometry is anisotropic, we discuss the case in elliptical coordinates (ρ, ξ) or ellipsoidal coordinates (ρ, ξ, η). Here, although two dimensions and three dimensions are different, we can remove the terms associated with η and x_3 to reduce three dimensions to two dimensions. The ellipsoidal coordinates (ρ, ξ, η) can be expressed as

$$\frac{x_1^2}{\rho + \lambda_{a1}^2} + \frac{x_2^2}{\rho + \lambda_{a2}^2} + \frac{x_3^2}{\rho + \lambda_{a3}^2} = 1, \qquad (6a)$$

$$\frac{x_1^2}{\xi + \lambda_{a1}^2} + \frac{x_2^2}{\xi + \lambda_{a2}^2} + \frac{x_3^2}{\xi + \lambda_{a3}^2} = 1, \qquad (6b)$$

$$\frac{x_1^2}{\eta + \lambda_{a1}^2} + \frac{x_2^2}{\eta + \lambda_{a2}^2} + \frac{x_3^2}{\eta + \lambda_{a3}^2} = 1, \qquad (6c)$$

where $\rho = \text{const}$ denotes an ellipsoidal surface, and λ_i is the semiaxis of the ellipsoid ($\rho = \text{const}$) along the x_i-axis. Accordingly, the Cartesian coordinates can be expressed as

$$x_1^2 = \frac{(\rho + \lambda_{a1}^2)(\xi + \lambda_{a1}^2)(\eta + \lambda_{a1}^2)}{(\lambda_{a1}^2 - \lambda_{a2}^2)(\lambda_{a1}^2 - \lambda_{a3}^2)}, \qquad (7a)$$

$$x_2^2 = \frac{(\rho + \lambda_{a2}^2)(\xi + \lambda_{a2}^2)(\eta + \lambda_{a2}^2)}{(\lambda_{a2}^2 - \lambda_{a1}^2)(\lambda_{a2}^2 - \lambda_{a3}^2)}, \qquad (7b)$$

$$x_3^2 = \frac{(\rho + \lambda_{a3}^2)(\xi + \lambda_{a3}^2)(\eta + \lambda_{a3}^2)}{(\lambda_{a3}^2 - \lambda_{a1}^2)(\lambda_{a3}^2 - \lambda_{a2}^2)}. \qquad (7c)$$

In the presence of an external linear thermal field $\boldsymbol{G}_0$ along the x_i-axis, the temperature profiles in different regions can be expressed as [22]

$$T_a = u_a x_i, \qquad (8a)$$

$$T_b = \left[u_b + v_b \int_{\rho_a}^{\rho} \frac{\mathrm{d}\rho}{(\rho + \lambda_{ai}^2)g(\rho)} \right] x_i, \qquad (8b)$$

$$T_c = \left[u_c + v_c \int_{\rho_a}^{\rho} \frac{\mathrm{d}\rho}{(\rho + \lambda_{ai}^2)g(\rho)} \right] x_i, \qquad (8c)$$

$$T_d = \left[u_d + v_d \int_{\rho_a}^{\rho} \frac{\mathrm{d}\rho}{(\rho + \lambda_{ai}^2)g(\rho)} \right] x_i, \qquad (8d)$$

where $g(\rho) = \sqrt{(\rho + \lambda_{a1}^2)(\rho + \lambda_{a2}^2)(\rho + \lambda_{a3}^2)} = \lambda_1 \lambda_2 \lambda_3$, and ρ_a ($= 0$) denotes the ellipsoidal core surface with semiaxes λ_{ai}. As we have explained above, $g(\rho) = \sqrt{(\rho + \lambda_{a1}^2)(\rho + \lambda_{a2}^2)} = \lambda_1 \lambda_2$ for two dimensions.

We use two mathematical properties to proceed. The first one is associated with the temperature derivations in eq. (8),

$$\frac{\partial x_i}{\partial \rho} = \frac{x_i}{2(\rho + \lambda_{ai}^2)}, \qquad (9a)$$

$$\frac{\partial}{\partial \rho} \left[x_i \int_{\rho_a}^{\rho} \frac{\mathrm{d}\rho}{(\rho + \lambda_{ai}^2)g(\rho)} \right] = \frac{x_i}{(\rho + \lambda_{ai}^2)g(\rho)}$$
$$+ \frac{x_i}{2(\rho + \lambda_{ai}^2)} \int_{\rho_a}^{\rho} \frac{\mathrm{d}\rho}{(\rho + \lambda_{ai}^2)g(\rho)}. \qquad (9b)$$

The second one is related to the integrations in eqs. (8b)–(8d) which can be rewritten as

$$\int_{\rho_a}^{\rho} \frac{\mathrm{d}\rho}{(\rho + \lambda_{ai}^2)g(\rho)} = \int_{\rho_a}^{\infty} \frac{\mathrm{d}\rho}{(\rho + \lambda_{ai}^2)g(\rho)}$$
$$- \int_{\rho}^{\infty} \frac{\mathrm{d}\rho}{(\rho + \lambda_{ai}^2)g(\rho)} = \frac{2L_{ai}}{g(\rho_a)} - \frac{2L_i}{g(\rho)}, \qquad (10a)$$

$$L_{ai} = \frac{g(\rho_a)}{2} \int_{\rho_a}^{\infty} \frac{\mathrm{d}\rho}{(\rho + \lambda_{ai}^2)g(\rho)}, \qquad (10b)$$

$$L_i = \frac{g(\rho)}{2} \int_{\rho}^{\infty} \frac{\mathrm{d}\rho}{(\rho + \lambda_{ai}^2)g(\rho)}, \qquad (10c)$$

where L_{ai} and L_i are shape factors along the x_i-axis.

Then, the boundary conditions can be expressed as

$$u_a = u_b, \qquad (11a)$$

$$u_b + v_b \int_{\rho_a}^{\rho_b} \frac{\mathrm{d}\rho}{(\rho + \lambda_{ai}^2)g(\rho)} =$$
$$u_c + v_c \int_{\rho_a}^{\rho_b} \frac{\mathrm{d}\rho}{(\rho + \lambda_{ai}^2)g(\rho)}, \qquad (11b)$$

$$u_c + v_c \int_{\rho_a}^{\rho_c} \frac{\mathrm{d}\rho}{(\rho + \lambda_{ai}^2)g(\rho)} =$$
$$u_d + v_d \int_{\rho_a}^{\rho_c} \frac{\mathrm{d}\rho}{(\rho + \lambda_{ai}^2)g(\rho)}, \qquad (11c)$$

$$\kappa_a u_a = \kappa_b \left[u_b + \frac{2v_b}{g(\rho_a)} \right], \qquad (11d)$$

$$\kappa_b \left[u_b + \frac{2v_b}{g(\rho_b)} + v_b \int_{\rho_a}^{\rho_b} \frac{\mathrm{d}\rho}{(\rho + \lambda_{ai}^2)\, g(\rho)} \right] =$$
$$\kappa_c \left[u_c + \frac{2v_c}{g(\rho_b)} + v_c \int_{\rho_a}^{\rho_b} \frac{\mathrm{d}\rho}{(\rho + \lambda_{ai}^2)\, g(\rho)} \right], \qquad (11e)$$

$$\kappa_c \left[u_c + \frac{2v_c}{g(\rho_c)} + v_c \int_{\rho_a}^{\rho_c} \frac{\mathrm{d}\rho}{(\rho + \lambda_{ai}^2)\, g(\rho)} \right] =$$
$$\kappa_d \left[u_d + \frac{2v_d}{g(\rho_c)} + v_d \int_{\rho_a}^{\rho_c} \frac{\mathrm{d}\rho}{(\rho + \lambda_{ai}^2)\, g(\rho)} \right], \qquad (11f)$$

$$u_d = G_0, \qquad (11g)$$

$$v_d = 0, \qquad (11h)$$

$$u_a = u_d. \qquad (11i)$$

The physical understanding of eq. (11) is similar to eq. (2). Similarly, we can derive two groups of thermal conductivities as

$$\kappa_b^{(1)} = \beta^{(1)}(\kappa_a, \kappa_d, \lambda_{ai}, \lambda_{bi}, \lambda_{ci}), \qquad (12a)$$

$$\kappa_c^{(1)} = \gamma^{(1)}(\kappa_a, \kappa_d, \lambda_{ai}, \lambda_{bi}, \lambda_{ci}), \qquad (12b)$$

or

$$\kappa_b^{(2)} = \beta^{(2)}(\kappa_a, \kappa_d, \lambda_{ai}, \lambda_{bi}, \lambda_{ci}), \qquad (13a)$$

$$\kappa_c^{(2)} = \gamma^{(2)}(\kappa_a, \kappa_d, \lambda_{ai}, \lambda_{bi}, \lambda_{ci}), \qquad (13b)$$

where $\beta^{(1)}$, $\gamma^{(1)}$ ($< \beta^{(1)}$), $\beta^{(2)}$, and $\gamma^{(2)}$ ($> \beta^{(2)}$) are four functions determined by eq. (11). The physical understanding of eqs. (12) and (13) is consistent with that of eqs. (3) and (4). The isotropic case with eqs. (3) and (4) is very complicated, let alone the anisotropic case with eqs. (12) and (13). Therefore, we use Mathematica to calculate thermal conductivities with determined $(\kappa_a, \kappa_d, \lambda_{ai}, \lambda_{bi}, \lambda_{ci})$ when performing simulations. Certainly, the anisotropic case with eqs. (12) and (13) can be reduced to the isotropic case with eqs. (3) and (4). We do not start from eqs. (12) and (13) to derive eqs. (3) and (4) because eqs. (12) and (13) are too complicated to simplify.

Nonlinear thermotics: geometrically isotropic and anisotropic cases. – We discuss the thermally nonlinear case where thermal conductivity is temperature-dependent. Such a consideration is necessary because many common materials are nonlinear such as silicon and germanium. We suppose the thermal conductivity of the matrix to be $\kappa_d(T) = \kappa_d f(T)$, where $f(T)$ can be any temperature-dependent functions. Then, we prove that the bilayer scheme can also be applied for thermally nonlinear cases as long as the ratio between the nonlinear thermal conductivities of core and matrix is a temperature-independent constant, namely $\kappa_d(T)/\kappa_a(T) = \kappa_d/\kappa_a$. Therefore, the thermal conductivity of the core should be $\kappa_a(T) = \kappa_a f(T)$.

We directly substitute $\kappa_d(T)$ and $\kappa_a(T)$ into eqs. (3) and (4). Then, we can also derive two groups of $\kappa_b(T)$ and $\kappa_c(T)$ which satisfy

$$\kappa_b(T) = \kappa_b f(T), \qquad (14a)$$

$$\kappa_c(T) = \kappa_c f(T). \qquad (14b)$$

Here, superscripts are omitted because both groups of thermal conductivities satisfy this property. More generally, we substitute $\kappa_d(T)$ and $\kappa_a(T)$ into eqs. (12) and (13). $\kappa_b(T)$ and $\kappa_c(T)$ also satisfy

$$\kappa_b(T) = \beta[\kappa_a f(T), \kappa_d f(T), \lambda_{ai}, \lambda_{bi}, \lambda_{ci}] =$$
$$\beta[\kappa_a, \kappa_d, \lambda_{ai}, \lambda_{bi}, \lambda_{ci}]f(T) = \kappa_b f(T), \qquad (15a)$$

$$\kappa_c(T) = \gamma[\kappa_a f(T), \kappa_d f(T), \lambda_{ai}, \lambda_{bi}, \lambda_{ci}] =$$
$$\gamma[\kappa_a, \kappa_d, \lambda_{ai}, \lambda_{bi}, \lambda_{ci}]f(T) = \kappa_c f(T). \qquad (15b)$$

Such a property allows us to transform the nonlinear Laplace equation into the linear Laplace equation. Meanwhile, general solutions are consistent in different regions.
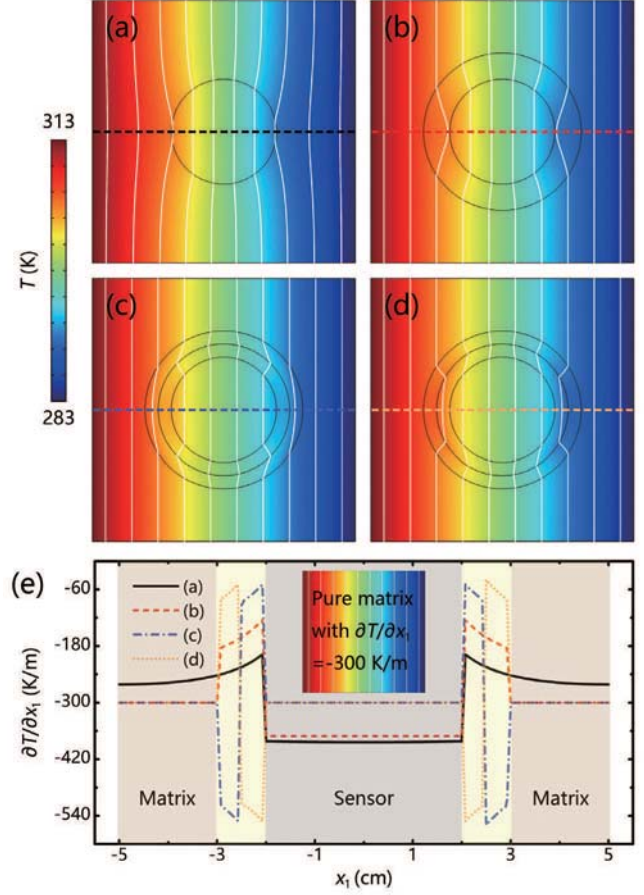

Fig. 2: Simulations of the geometrically isotropic case. (a) Sensor embedded in the matrix. (b) Sensor coated by the monolayer scheme proposed in ref. [12] with inner and outer radii of λ_a and λ_c, respectively. The thermal conductivity of the single layer is $161.1\,\mathrm{W\,m^{-1}\,K^{-1}}$. (c) Sensor coated by two layers designed with eq. (3). (d) Sensor coated by two layers designed with eq. (4). (e) Temperature gradients on the dashed lines in (a)–(d) as a function of x_1. The simulation size is $10 \times 10\,\mathrm{cm}^2$. The temperatures of the left and right boundaries are set at 313 and 283 K. The other boundaries are insulated. $\lambda_a = 2$, $\lambda_b = 2.5$, $\lambda_c = 3\,\mathrm{cm}$, and $\kappa_a = 50$, $\kappa_d = 100\,\mathrm{W\,m^{-1}\,K^{-1}}$. $\kappa_b^{(1)} = 378.5$, $\kappa_c^{(1)} = 58.5$, and $\kappa_b^{(2)} = 26.7$, $\kappa_c^{(2)} = 346.3\,\mathrm{W\,m^{-1}\,K^{-1}}$.

The nonlinear Laplace equation in different regions can be expressed as

$$\boldsymbol{\nabla} \cdot [-\kappa_{a,b,c,d}(T)\boldsymbol{\nabla}T] = \boldsymbol{\nabla} \cdot [-\kappa_{a,b,c,d}f(T)\boldsymbol{\nabla}T] =$$
$$\boldsymbol{\nabla} \cdot [-\kappa_{a,b,c,d}\boldsymbol{\nabla}h(T)] = 0, \qquad (16a)$$

where $\partial h(T)/\partial T = f(T)$. In other words, as long as we replace T with $h(T)$, the nonlinear Laplace equation can be transformed into the linear Laplace equation. Therefore, the above theories can be applied without any correction. The only assumption is that the ratio between the nonlinear thermal conductivities of sensor and matrix is a temperature-independent constant.
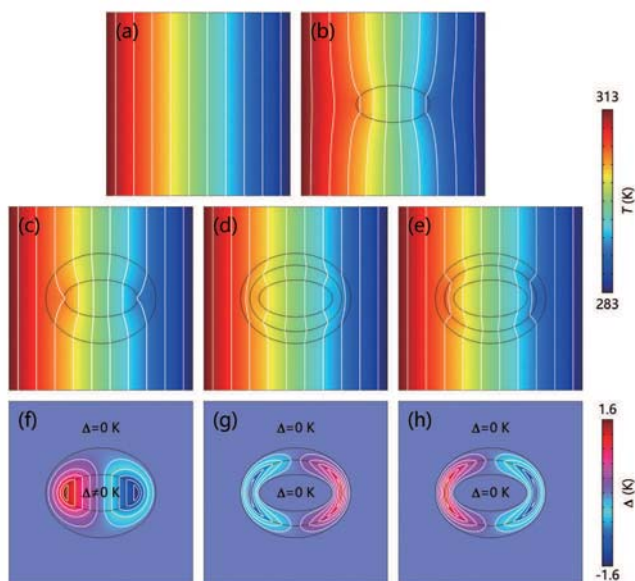
Fig. 3: Simulations of the geometrically anisotropic case. (a) Pure matrix. (b) Sensor embedded in the matrix. (c) Sensor coated by the monolayer scheme proposed in ref. [16] whose thermal conductivity is 149.5 W m^{-1} K^{-1}. (d) Sensor coated by two layers designed with eq. (12). (e) Sensor coated by two layers designed with eq. (13). (f) Temperature difference with the temperature in (c) minus that in (a). (g) Temperature difference with the temperature in (d) minus that in (a). (h) Temperature difference with the temperature in (e) minus that in (a). $\lambda_{a1} = 2$, $\lambda_{a2} = 1$, $\lambda_{b1} = 2.5$, $\lambda_{b2} = 1.8$, $\lambda_{c1} = 3$, $\lambda_{c2} = 2.45$ cm, and $\kappa_a = 5$, $\kappa_d = 100$ W m^{-1} K^{-1}. $\kappa_b^{(1)} = 274.5$, $\kappa_c^{(1)} = 61.8$, and $\kappa_b^{(2)} = 2.4$, $\kappa_c^{(2)} = 342.1$ W m^{-1} K^{-1}.
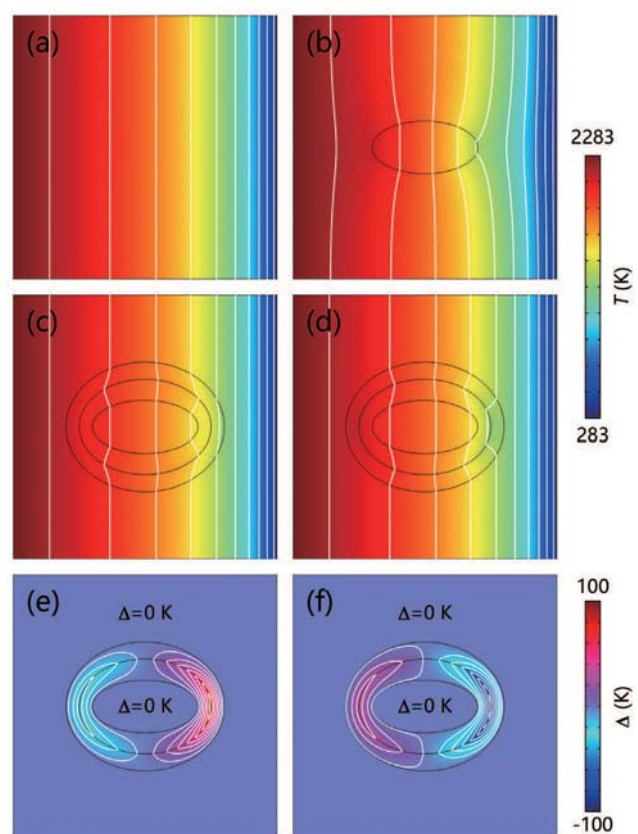

Fig. 4: Simulations of the thermally nonlinear case. The temperatures of the left and right boundaries are set at 2283 and 283 K, respectively. $f(T) = 1 + 10^{-9}T^3$. The other parameters are the same as those for fig. 3.

Linear and nonlinear thermotics: finite-element simulations. – We use the template of solid heat transfer in COMSOL MULTIPHYSICS [23] to confirm these theoretical analyses. Without loss of generality, we perform simulations in two dimensions.

Firstly, we discuss the geometrically isotropic case in fig. 2. A thermal sensor is embedded in the matrix for temperature detection. Since the thermal conductivity of the sensor is different from that of the matrix, the whole temperature profile is distorted (see fig. 2(a)). Therefore, the sensor is not only thermally visible but also inaccurate. When a pioneering monolayer scheme [12] is applied, it can ensure thermal invisibility, but it does not perform well in accuracy because the temperature in the sensor is still different from the original one (see fig. 2(b)). Then, we resort to the bilayer scheme. We coat the sensor with the bilayer scheme whose thermal conductivities are designed according to eq. (3), and the simulation result is shown in fig. 2(c). Clearly, the temperature in the matrix becomes linear again, thus making the sensor thermally invisible. Meanwhile, the temperature in the sensor is the same as the original one, thus ensuring accurate detection. We also design the thermal conductivities of the two layers according to eq. (4), and the same effect can

be obtained (see fig. 2(d)). For quantitative comparison, we export the data on the dashed lines in figs. 2(a)–(d). Since the temperature difference is not large enough to be observed, we export the temperature gradient $\partial T/\partial x_1$ for comparison. The result is presented in fig. 2(e), indicating that the bilayer scheme can indeed ensure thermal invisibility and accurate detection simultaneously. The inset of fig. 2(e) shows the temperature profile of a pure matrix with a linear thermal field of -300 K/m.

Then, we discuss the geometrically anisotropic case in fig. 3, which is more practical. The results are similar to the geometrically isotropic case. Figures 3(a) and (b) demonstrate the temperature profiles without and with a sensor embedded in the matrix, respectively. The sensor distorts the whole temperature profile, which results in thermal visibility and inaccurate detection of the sensor. When the monolayer scheme [16] is applied, it can ensure thermal invisibility, but the temperature in the sensor is still changed (see fig. 3(c)). Figures 3(d) and (e) show the results coated by two layers designed with eqs. (12) and (13), respectively. Again, the temperatures in the matrix and sensor become the same. Therefore, the sensor is thermally invisible and accurate. For clarity, we
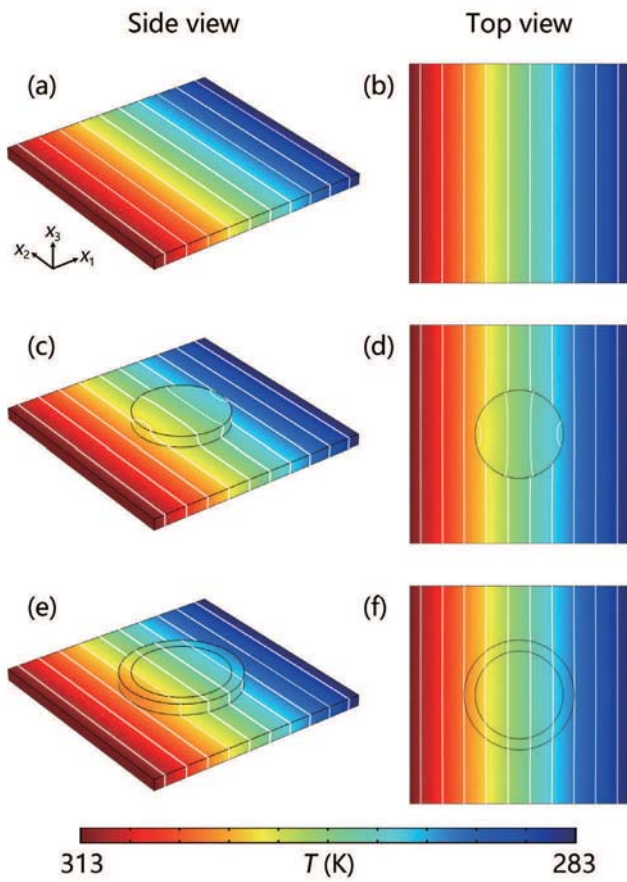
Fig. 5: Nondestructive detection. (a) and (b): Simulations of a pure matrix with thermal conductivity of $100\,\mathrm{W\,m^{-1}\,K^{-1}}$ and size of $10\times10\times0.5\,\mathrm{cm^3}$. (c) and (d): Simulations of the attachment of a sensor with thermal conductivity of $5\,\mathrm{W\,m^{-1}\,K^{-1}}$, radius of $2\,\mathrm{cm}$, and thickness of $0.5\,\mathrm{cm}$ on the upper surface of the matrix. (e) and (f): Simulations of a shell with thermal conductivity of $\mathrm{diag}(10^{-5},10^{-5},10^{5})\,\mathrm{W\,m^{-1}\,K^{-1}}$ (expressed in the Cartesian coordinates), radius of $2.5\,\mathrm{cm}$, and thickness of $0.5\,\mathrm{cm}$ coating the sensor.

plot the temperature difference Δ with the temperature in fig. 3(c) (fig. 3(d) or fig. 3(e)) minus that in fig. 3(a), which is shown in fig. 3(f) (fig. 3(g) or fig. 3(h)). Clearly, our scheme ensures that the temperature difference Δ in the matrix and sensor is always zero, confirming an accurate and thermally invisible sensor.

Finally, we discuss the thermally nonlinear case in fig. 4. Nonlinear (temperature-dependent) thermal conductivities, no matter weak or strong, are common in nature. Here, "strong" (or "weak") means that the nonlinear (or linear) term of thermal conductivity is dominant. Therefore, it is necessary to extend our scheme to thermally nonlinear cases. To make nonlinear properties clear, we discuss strong nonlinearity directly. A typical case of strong nonlinearity is thermal radiation with the Rosseland diffusion approximation, which is proportional to T^3 [24–26]. Therefore, we consider $f(T)=\mu+\nu T^3$, where μ and ν are two constants. We set a high temperature at

2283 K, and aerogel (or ceramic) which has excellent tolerance of high temperatures can be applied to observe thermal nonlinearity. As proved in eq. (15), we can directly multiply the original thermal conductivities with $f(T)$ to proceed.

Since the thermal conductivity of the matrix is nonlinear, the temperature gradient is no longer a constant (see fig. 4(a)). When an elliptical sensor is embedded in the matrix, the straight isotherms are distorted (see fig. 4(b)). Then, we coat the sensor with two layers designed with eq. (15). The simulation results are presented in figs. 4(c) and 4(d), respectively. Clearly, the distorted isotherms in the matrix and sensor are restored. Similarly, we also plot the temperature difference Δ with the temperature in fig. 4(c) (or fig. 4(d)) minus that in fig. 4(a), and the results are shown in fig. 4(e) (or fig. 4(f)). We can observe zero temperature difference Δ in the matrix and sensor, so the bilayer scheme performs with satisfaction.

Discussion and conclusion. – For temperature detection, a thermal sensor is embedded in the matrix, which may cause matrix destruction. Therefore, developing nondestructive detection is one future direction, which only requires surface attachment. Here, we make a preliminary attempt to design nondestructive detection. The similarity is that both schemes aim to make a thermal sensor accurate and invisible. The difference is that the former should embed a sensor in the matrix, and the latter only requires surface attachment. For this purpose, we consider a thin three-dimensional model. Figures 5(a) and (b) show the results of a pure matrix with a linear thermal gradient. When a sensor is put on its upper surface, the detected temperature in the sensor is no longer the original one, making temperature detection inaccurate (see figs. 5(c) and (d)). With the assistance of a coating shell, the distorted temperature in the sensor is restored, thus making temperature detection accurate again (see figs. 5(e) and (f)). These results may encourage further explorations on nondestructive detection and advance temperature detection.

We discuss the bilayer scheme in stable regimes, which can also be extended to transient regimes by taking heat capacity and density into consideration [27–29]. Since invisibility is a special case of camouflage, these results also provide guidance to thermal camouflage [30–43]. When performing experiments, the required parameters can be obtained with common materials such as copper and steel. Nevertheless, the present scheme is dependent on elliptical/ellipsoid shapes with which the Laplace equation can be analytically expanded. Therefore, other methods remain to be explored for complex shapes [44], such as combining neutral inclusion [10] and transformation thermotics [45–48].

In summary, we have proposed a bilayer scheme to design thermally invisible sensors. Compared with existing schemes, the present one is not only accurate but also applicable for geometrically anisotropic cases and thermally

nonlinear cases. Thermal invisibility can protect sensors from being detected, and accurate detection is beneficial to practical applications. The extensions to geometric anisotropy and thermal nonlinearity make thermal sensors more widely applicable. Moreover, we unify two/three-dimensional cases, isotropic/anisotropic cases, and linear/nonlinear cases with a single theoretical framework, which lays a solid foundation to design thermal metamaterials under different conditions.

$$* * *$$

REFERENCES

[1] Alú A. and Engheta N., *Phys. Rev. Lett.*, **102** (2009) 233901.
[2] Greenleaf A., Kurylev Y., Lassas M. and Uhlmann G., *Phys. Rev. E*, **83** (2011) 016603.
[3] Zhu X. F., Liang B., Kan W. W., Zou X. Y. and Cheng J. C., *Phys. Rev. Lett.*, **106** (2011) 014301.
[4] Fleury R., Soric J. and Alú A., *Phys. Rev. B*, **89** (2014) 045122.
[5] Fleury R., Sounas D. and Alú A., *Nat. Commun.*, **6** (2015) 5905.
[6] Mach-Batlle R., Navau C. and Sanchez A., *Appl. Phys. Lett.*, **112** (2018) 162406.
[7] Chen P.-Y., Soric J. and Alú A., *Adv. Mater.*, **24** (2012) OP281.
[8] Farhat M., Chen P.-Y., Bagci H., Amra C., Guenneau S. and Alú A., *Sci. Rep.*, **5** (2015) 9876.
[9] Farhat M., Guenneau S., Chen P.-Y., Alú A. and Salama K. N., *Phys. Rev. Appl.*, **11** (2019) 044089.
[10] He X. and Wu L. Z., *Phys. Rev. E*, **88** (2013) 033201.
[11] Shen X. Y. and Huang J. P., *Int. J. Heat Mass Transfer*, **78** (2014) 1.
[12] Yang T. Z., Bai X., Gao D. L., Wu L. Z., Li B. W., Thong J. T. L. and Qiu C.-W., *Adv. Mater.*, **27** (2015) 7752.
[13] Xu H. Y., Shi X. H., Gao F., Sun H. D. and Zhang B. L., *Phys. Rev. Lett.*, **112** (2014) 054301.
[14] Han T. C., Bai X., Gao D. L., Thong J. T. L., Li B. W. and Qiu C.-W., *Phys. Rev. Lett.*, **112** (2014) 054302.
[15] Ma Y. G., Liu Y. C., Raza M., Wang Y. D. and He S. L., *Phys. Rev. Lett.*, **113** (2014) 205501.
[16] Han T. C., Yang P., Li Y., Lei D. Y., Li B. W., Hippalgaonkar K. and Qiu C.-W., *Adv. Mater.*, **117** (2018) 1804019.
[17] Li Y., Zhu K.-J., Peng Y.-G., Li W., Yang T. Z., Xu H. X., Chen H., Zhu X.-F., Fan S. H. and Qiu C.-W., *Nat. Mater.*, **18** (2019) 48.
[18] Xu G. Q., Zhou X. and Zhang J. Y., *Int. J. Heat Mass Transfer*, **142** (2019) 118434.

[19] Xu L. J. and Huang J. P., *EPL*, **125** (2019) 64001.
[20] Yang S., Xu L. J. and Huang J. P., *EPL*, **128** (2019) 34002.
[21] Yang S., Xu L. J. and Huang J. P., *EPL*, **126** (2019) 54001.
[22] Milton G. W., *The Theory of Composites*, Vol. **124** (Cambridge University Press, Cambridge) 2004.
[23] http://www.comsol.com/.
[24] Xu L. J. and Huang J. P., *Phys. Rev. Appl.*, **12** (2019) 044048.
[25] Xu L. J. Dai G. L. and Huang J. P., *Phys. Rev. Appl.*, **13** (2020) 024063.
[26] Su C., Xu L. J. and Huang J. P., *EPL*, **130** (2020) 34001.
[27] Yang T. Z., Su Y. S., Xu W. K. and Yang X. D., *Appl. Phys. Lett.*, **109** (2016) 121905.
[28] Liu Y. X., Guo W. L. and Han T. C., *Int. J. Heat Mass Transfer*, **115** (2017) 1.
[29] He X., Yang T. Z. and Zhang X. W., *Sci. Rep.*, **7** (2017) 16671.
[30] Hu R., Zhou S. L., Li Y., Lei D. Y., Luo X. B. and Qiu C.-W., *Adv. Mater.*, **30** (2018) 1707237.
[31] Li Y., Bai X., Yang T. Z., Luo H. L. and Qiu C.-W., *Nat. Commun.*, **9** (2018) 273.
[32] Hu R., Huang S. Y., Wang M., Zhou L. L., Peng X. Y. and Luo X. B., *Phys. Rev. Appl.*, **10** (2018) 054032.
[33] Hu R., Huang S. Y., Wang M., Luo X. L., Shiomi J. and Qiu C.-W., *Adv. Mater.*, **31** (2019) 1807849.
[34] Xu L. J., Yang S. and Huang J. P., *Phys. Rev. Appl.*, **11** (2019) 054071.
[35] Xu L. J., Yang S. and Huang J. P., *Phys. Rev. E*, **100** (2019) 062108.
[36] Huang S. Y., Zhang J. W., Wang M., Lan W., Hu R. and Luo X. B., *ES Energy Environ.*, **6** (2019) 51.
[37] Yang F. B., Xu L. J. and Huang J. P., *ES Energy Environ.*, **6** (2019) 45.
[38] Hu R., Song J. L., Liu Y. D., Xi W., Zhao Y. T., Yu X. J., Cheng Q., Tao G. M. and Luo X. B., *Nano Energy*, **72** (2020) 104687.
[39] Song J. L., Huang S. Y., Ma Y. P., Cheng Q., Hu R. and Luo X. B., *Opt. Express*, **28** (2020) 875.
[40] Peng Y.-G., Li Y., Cao P.-C., Zhu X.-F. and Qiu C.-W., *Adv. Funct. Mater.*, **30** (2020) 2002061.
[41] Xu L. J., Yang S., Dai G. L. and Huang J. P., *ES Energy Environ.*, **7** (2020) 65.
[42] Xu L. J. and Huang J. P., *Sci. China-Phys. Mech. Astron.*, **63** (2020) 228711.
[43] Liu Y. D., Song J. L., Zhao W. X., Ren X. C., Cheng Q., Luo X. B., Fang N. X. L. and Hu R., *Nanophotonics*, **9** (2020) 855.
[44] Ji Q., Chen X., Fang, G., Liang J., Yan X., Laude V. and Kadic M., *AIP Adv.*, **9** (2019) 045029.
[45] Fan C. Z., Gao Y. and Huang J. P., *Appl. Phys. Lett.*, **92** (2008) 251907.
[46] Chen T. Y., Weng C.-N. and Chen J.-S., *Appl. Phys. Lett.*, **93** (2008) 114103.
[47] Guenneau S., Amra C. and Veynante D., *Opt. Express*, **20** (2012) 8207.
[48] Schittny R., Kadic M., Guenneau S. and Wegener M., *Phys. Rev. Lett.*, **110** (2013) 195901.